ARTICLE IN PRESS

Nuclear Inst. and Methods in Physics Research, A ▮ (▮▮▮▮) ▮▮▮–▮▮▮

Contents lists available at ScienceDirect

Nuclear Inst. and Methods in Physics Research, A

journal homepage: www.elsevier.com/locate/nima

Timing layers, 4- and 5-dimension tracking

N. Cartiglia [a,*], R. Arcidiacono [a,b], M. Ferrero [a], M. Mandurrino [a], H.-F.W. Sadrozinski [c], V. Sola [a,d], A. Staiano [a], A. Seiden [c]

[a] INFN, Torino, Italy
[b] Università del Piemonte Orientale, Italy
[c] SCIPP, University of California Santa Cruz, CA, USA
[d] Università di Torino, Torino, Italy

ARTICLE INFO

MSC:
XX-XX
XX-XX

Keywords:
Silicon
Fast detector
Low gain
Charge multiplication
LGAD

ABSTRACT

The combination of precision space and time information in particle tracking, the so called 4D tracking, is being considered in the upgrade of the ATLAS, CMS and LHCb experiments at the High-Luminosity LHC, set to start data taking in 2024–2025. Regardless of the type of solution chosen, space–time tracking brings benefits to the performance of the detectors by reducing the background and sharpening the resolution; it improves tracking performances and simplifies tracks combinatorics. Space–time tracking also allows investigating new physics channels, for example it opens up the possibilities of new searches in long-living particles by measuring accurately the time of flight between the production and the decay vertexes. The foreseen applications of 4D tracking in experiments with very high acquisition rates, for example at HL-LHC, add one more dimension to the problem, increasing dramatically the complexity of the read-out system and that of the whole detector design: we call 5D tracking the application of 4D tracking in high rate environments.

1. Introduction

The accurate measurement of the time of passage of particles has been used extensively in high-energy particle experiments to distinguish particles on the assumption that heavier particles have lower velocities. However, in the high luminosity update of the LHC accelerator (HL-LHC [1]), timing information will be used in a radically new way: timing and tracking detectors will perform a joint reconstruction of the passage of particles in space and time to be able to cope with the very high density of particles.

As a first example, consider the situation of the CMS [2,3] and ATLAS [4,5] experiments at HL-LHC: at each bunch crossing, between 150 and 200 pairs of protons will collide in a time window of about $\Delta t = 150$ ps, generating thousands of particles. Under these conditions, traditional particle tracking faces severe challenges; it has been estimated that between 10 and 15% [6] of the vertexes recognized by the tracking devices as a single vertex are actually composed by two vertexes overlapping in space so tightly that cannot be resolved. A second example can be taken from similar studies performed by the LHCb [7] experiment that have demonstrated, among many other results, a degradation of a factor of 10 (from 1% to 13%) [8] in assigning the beauty and charm hadrons to their correct primary vertex, impairing the LHCb capability of performing its physics program.

Timing detectors will exploit the time spread between interactions to correctly disentangle spatially overlapping events, aiding the tracker devices in the correct reconstruction of each event: the inclusion of the timing information in the event reconstruction can almost fully offset the increased particle density foreseen at HL-LHC, recovering at HL-LHC the same performances enjoyed currently by the LHC experiments, albeit at much lower luminosity [9].

Timing detectors are extremely specialized sensors, and each operating condition and geometry requires a different choice of optimum technology. Depending on the sensor that will be used, timing information can be available at different stages in the reconstruction of an event. The best option is when timing is associated to each point of the track. This is the current proposal of the LHCb collaboration that foresees a time-tracking device based on 3D trench silicon sensors with a 100 μm pitch combined with a time resolution of 100 ps, able to withstand fluences between $10^{16} - 10^{17}$ 1 MeV n_{eq} cm^{-2} .

The ATLAS and CMS collaborations have instead adopted the approach of assigning to each track, and not to each hit, a timing information. Since this approach has fewer measuring points, the precision per point needs to be higher, in the range of 30–40 ps. Within this underlying common detector philosophy, the choices of CMS and ATLAS differ significantly: CMS has decided to design a single-layer detector in the pseudo-rapidity range $0 < \eta < 3$. In the central region, given the large area and low radiation environment, are used crystals coupled with SiPM; in the forward part, $1.6 < \eta < 3$, where fluences are up to $1.5 \cdot 10^{15}$ 1 MeV n_{eq} cm^{-2}, are used Ultra Fast Silicon Detectors (UFSD) [10–13]

* Corresponding author.
E-mail address: cartiglia@to.infn.it (N. Cartiglia).

https://doi.org/10.1016/j.nima.2018.09.157
Received 25 February 2018; Received in revised form 20 September 2018; Accepted 28 September 2018
Available online xxxx
0168-9002/

with 3 mm^2 pads. ATLAS, on the other hand, has opted for a 2-layer detector, also based on UFSD sensors, with 1.9 mm^2 pads covering the pseudo-rapidity range $2.4 < \eta < 4$. Given the higher rapidity coverage, the ATLAS detector will need to withstand higher radiation levels, with fluences reaching $5 \cdot 10^{15}$ 1 MeV n_{eq} cm^{-2} and, at the highest rapidity, an equal proton fluence.

2. Signal formation and time-tagging: aide-memoire

In every particle detector, the shape of the induced current signal can be calculated using Ramo–Shockley theorem [14,15] that states that the current induced by a charge carrier is proportional to its electric charge q, the drift velocity v and the weighting field E_w:

$$i = qvE_w. \quad (1)$$

This simple equation has important implications for timing detectors since the shape of the current i, to obtain a good time resolution, needs always to be the same, regardless of where the impinging particle hits the sensor: (i) the drift velocity needs to be constant throughout the volume of the sensor, (ii) the carriers should always move with saturated drift velocity, and (iii) the weighting field E_w should not vary along the electrode pitch. These facts indicate that to obtain a good time resolution the sensor should have a geometry as close as possible to that of a parallel plate capacitor, with uniform electric and weighting fields: implants need to have a width very similar to the pitch, and the implant pitch needs to be larger than the sensor thickness.

The timing capabilities of silicon sensors can be explored by modeling the sensor as a capacitor (C_{Det}) with a current source in parallel, readout by a pre-amplifier that shapes the signal. The pre-amplifier output is then compared to a fixed threshold (V_{Th}) to determine the time of arrival. The time resolution σ_t can be expressed as the sum of several terms: (i) Jitter, (ii) Fluctuations of the ionization process producing shape and amplitude variations, (iii) signal distortion, and (iv) TDC binning:

$$\sigma_t^2 = \sigma_{Jitter}^2 + (\sigma_{Local\ ionization} + \sigma_{Total\ ionization})^2 + \sigma_{Distortion}^2 + \sigma_{TDC}^2. \quad (2)$$

Let us analyze the last 3 terms (see [10] for details) of Eq. (2):

- We consider the effect of different signal amplitudes $\sigma_{Total\ ionization}$, the so-called time walk effect, compensated by an appropriate electronic circuit (either Constant Fraction Discriminator or Time over Threshold).
- The $\sigma_{Distortion}^2$ term is due to two factors: non-uniform weighting field, and non-saturated drift velocity. Both terms are reduced to be small contributions by using a "parallel plate geometry" and operating the sensor at a bias voltage where the carriers' velocity is saturated.
- We assume a TDC binning of 20–30 ps, similar to what is currently assumed by the CMS collaboration for its timing layer.

For the reasons listed above, the last 3 terms of Eq. (2) can be considered non-leading contributions to the total value of the time resolution, each term contributing less than 10 ps in quadrature. Let us now analyze the first two terms:

- the electronic jitter term is given by the ratio of the electronic noise N over the signal slew rate dV/dt, $\sigma_t(jitter) = N/(dV/dt)$: larger signals, for constant noise, have smaller jitter;
- the signal variations due to the non-uniform creation of electron–hole pairs along the particle path, the *Landau noise*, is due to the physics of the ionization process, and it cannot be avoided.

3. A new paradigm: controlled low-gain in silicon detectors

The *Low Gain Avalanche Diode* design is a concept in silicon detector design that merges some advantages of the standard silicon sensors with the main feature of APDs. The overarching idea is to design silicon detectors with signals that are large enough to assure excellent timing performance while keeping the gain as low as possible. The design has been introduced by the Centro Nacional de Microelectrónica (CNM) Barcelona [16], followed by the Fondazione Bruno Kessler (FBK) [17] and Hamamatsu Photonics [18].

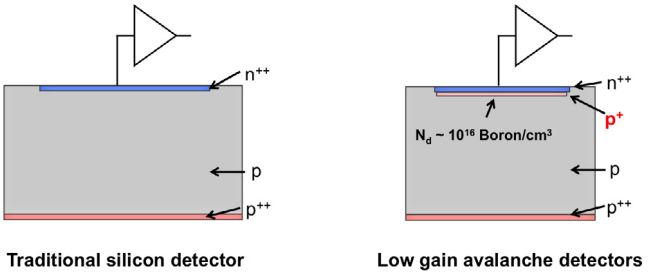

Fig. 1. Schematic of a traditional silicon diode (left) and of a Low-Gain Avalanche Diode (right). The additional p^+ layer underneath the n^{++} electrode creates, when depleted, a large electric field that generates charge multiplications.

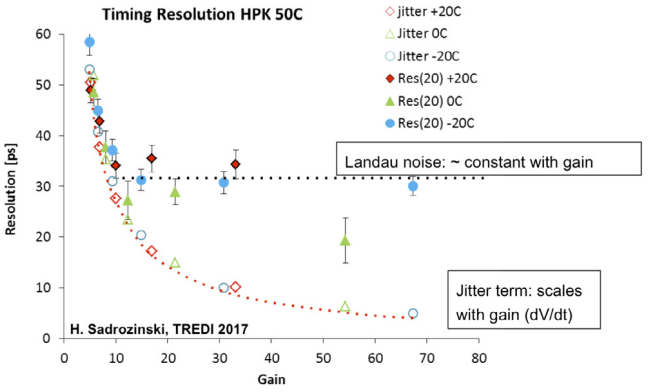

Fig. 2. Variation of the jitter and total time resolution as a function of the UFSD gain, as measured on a Hamamatsu 50-micron thick UFSD sensor: the jitter term, calculated as $\sigma_t(jitter) = N/(dV/dt)$, decreases constantly with gain while the total time resolution flattens around $\sigma_t(Total) = 30$ ps.

Charge multiplication in silicon sensors happens when the charge carriers are in electric fields of the order of $E \sim 300$ kV/cm: the additional doping layer present at the $n-p$ junction in the LGAD design, Fig. 1, generates the high field necessary to achieve charge multiplication. In the following, we will use the name of "Ultra-Fast Silicon Detectors" (UFSD) to indicate LGAD sensors optimized for timing performances. UFSD sensors have the advantage of having a large signal dV/dt and therefore are able to minimize jitter. The thickness of the gain layer is of the order of 1 μm.

The Landau noise, instead, depends strongly on the sensor thickness, and moderately on the gain value. Fig. 2 [19] shows the variation of these two terms as a function of the UFSD gain, as measured on a Hamamatsu 50-micron thick UFSD sensor: the jitter term, calculated as $\sigma_t(jitter) = N/(dV/dt)$, decreases constantly with gain while the total time resolution flattens to a value of 30–35 ps when the gain is about 20–25.

4. Evolution of UFSD sensors for the ATLAS and CMS timing layers

The design of UFSD sensors is evolving rapidly, mostly driven by the requests of the ATLAS and CMS collaborations for the construction of their timing layers. ATLAS needs to produce ~ 9k sensors of 2×4 cm^2, each sensor with 450 1.3×1.3 mm^2 pads while CMS aims at producing ~ 3k sensors of 4.8×9.6 cm^2, each sensor with 1536 1×3 mm^2 pads, a sketch of the sensors is shown in Fig. 3. The most important areas of R&D [18,20–23] are (i) radiation damage , (ii) gain uniformity, (iii)

Please cite this article in press as: N. Cartiglia, et al., Timing layers, 4- and 5-dimension tracking, Nuclear Inst. and Methods in Physics Research, A (2018), https://doi.org/10.1016/j.nima.2018.09.157.

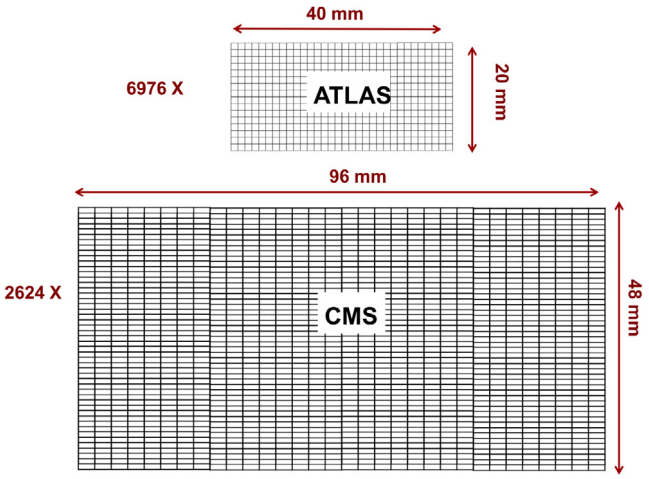

Fig. 3. Sketch of the ATLAS and CMS UFSD sensors for their respective timing layer.

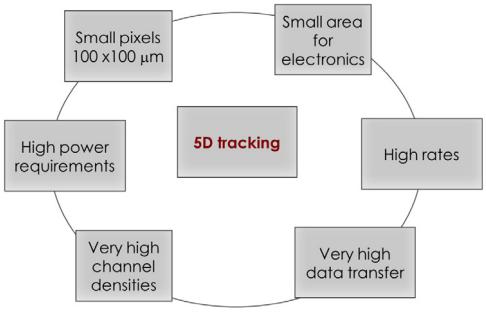

Fig. 4. Interconnection of several aspects of space–time tracking at high rate.

sensor size and (iv) fill factor. To this end, several productions of UFSD are planned by 3 foundries (CNM, FBK and HPK) in the next couple of years, with the goal of reaching reliable production of at least ~5×5 cm^2 sensors, with 1- 2k pixels, a fill factor exceeding 95%, and a time resolution of ~ 35 ps up to fluences above 10^{15} 1 MeV n_{eq} cm^{-2} and better of ~ 60 ps up to fluences of 10^{16} 1 MeV n_{eq} cm^{-2}.

5. 5-Dimension tracking: measuring space–time coordinates at high rate

UFSD with appropriate electronics are able to provide accurately space–time coordinates, however, in many experiments, an additional fact actually constrains the design of the detector: particles rate: it is a key factor in the overall detector, as it impacts the front-end real estate, power consumption and data transfer, see sketch in Fig. 4. For this reason, we consider rate as an additional dimension with respect of 4D tracking.

Let us consider a standard pixel of 100 × 100 μm^2: fitting the necessary electronics in the corresponding real-estate on the read-out chip, in environments with high particle rates, is very challenging. The measurement of time needs several basic blocks such as a pre-amplifier, a comparator and a TDC however, at a high rate, the TDC digitization speed might not be enough to keep up with the particle rate, and more than one TDC is needed per each pixel. Therefore, the particles rate has a direct impact on the minimum dimension of each pixel, as Fig. 5 shows [24,25]: in the 130 nm technological node a TDC needs approximately ~100×100 μm^2, that scales to ~50×50 μm^2 in the 65 nm technological node, and hopefully, to ~25×25 μm^2 in the 28 nm node. High rate and small pixel size, therefore, require the use of the smallest possible technological node available.

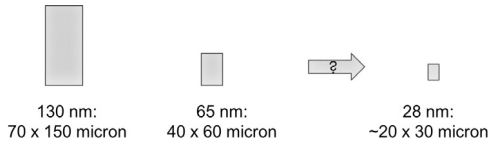

Fig. 5. Scaling of TDC sizes with the technological node.

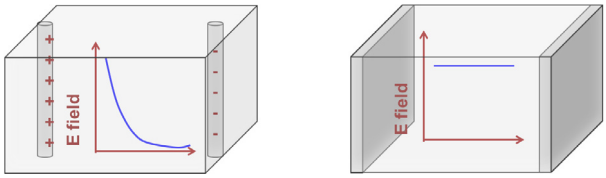

Fig. 6. Left side: 3D column sensors have electric and weighting fields changing rapidly with the position. Right side: 3D trench sensors have parallel plate-like geometry, with constant fields ideal for timing measurements.

The situation is further complicated by the large amount of data volume generated by several TDCs working in parallel in each pixel, and by the need to remove the power used by the analog front-end and digital electronics. Of equal importance, but not discussed in this article, are the new algorithms and read-out architectures, as those presented in [26], needed to fully exploit 5D-tracking,

6. 3D trench detectors for timing measurements

3D silicon sensors are well known for their radiation resistance, and they are currently used successfully in the ATLAS inner pixel layer [27]. It has also been suggested in [28] that 3D sensors with trench geometry might have very good time resolution. Fig. 6 shows the reason for this claim: while the 3D column geometry (left side) has both electric and weighting fields changing rapidly and therefore does not provide the constant signals needed to achieve a good time resolution, the 3D trench geometry (right side) has, due to its parallel plate geometry, constant electric and weighting fields ideal for timing measurements.

Fig. 7 shows the simulation, performed with the Weightfield2 program [29], of the signals generated in a 3D trench detectors by a laser impulse for two positions in the cell, for a new sensors (center) and after a fluence of 10^{16} 1 MeV n_{eq} cm^{-2} (right side). The detector has a spacing of 50 μm between electrodes, it is 200 μm thick, and the applied voltage is 200 V when not irradiated. For a new detector the total charge is 2.2 fC, while for the irradiated case it is reduced to 1 fC due to charge trapping.

Fig. 7 shows that in a non-irradiated 3D trench sensor, the current generated by the electrons is constant till it goes sharply to zero when the electrons reach their collecting electrode; the same effect is true also for holes, albeit with a lower current. The difference in height and length between the electrons and holes currents reflect their different mobility. An interesting feature of the signal in 3D trench detectors is that the overall current pulse length depends on the particle impinging position: it is minimal when the particle passes near the anode, and maximal when it is near the cathode. After a fluence of 10^{16} 1 MeV n_{eq} cm^{-2} the sensor needs to be biased to a much higher voltage (V_{Bias} ~ 500 V) in order to deplete the bulk and have good carriers velocity; the current is drastically reduced by charge trapping, as shown in the right side of Fig. 7. Above fluences of $2-3\cdot10^{16}$ 1 MeV n_{eq} cm^{-2}, the electric field needed to deplete 50 μm is above the onset of gain in the bulk, rapidly reaching breakdown values. For this reason, smaller cell sizes are needed when using 3D sensors in very high radiation environments. Remarkably, the current signal generated by a particle in a sensor with

Please cite this article in press as: N. Cartiglia, et al., Timing layers, 4- and 5-dimension tracking, Nuclear Inst. and Methods in Physics Research, A (2018), https://doi.org/10.1016/j.nima.2018.09.157.

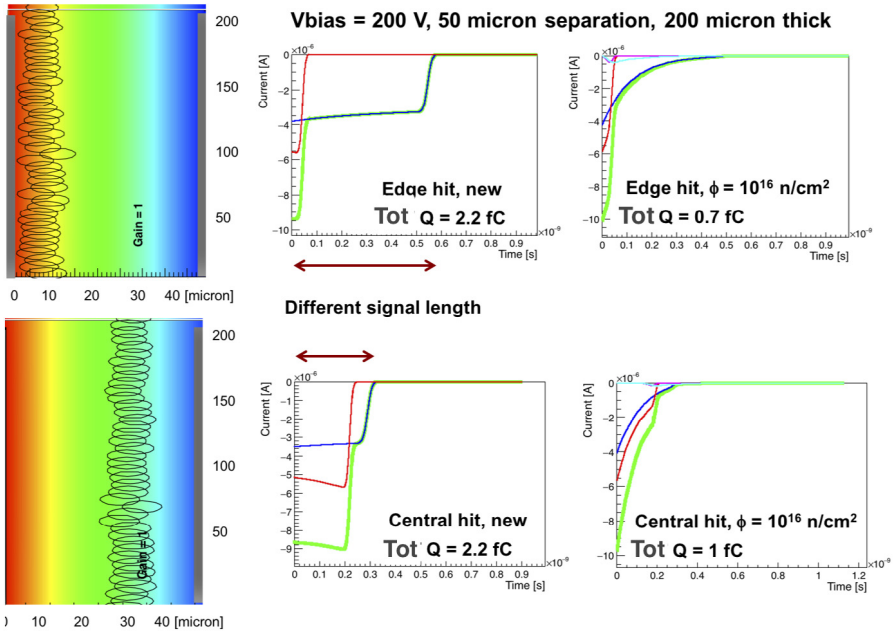

Fig. 7. Left side: electric potential in a 3D trench detector. Center: current signal in a new sensor, right side: current signal in a sensor irradiated to 10^{16} 1 MeV n_{eq} cm^{-2}.

3D trench geometry should not suffer from Landau fluctuations since uniformly-distributed or clustered charges induce the same current on the electrodes.

7. Outlook

The concurrent measurement of space and time in high energy physics experiment is attracting a lot of attention due to the need to overcame very high pile-up rate at HL-LHC and the recent development in silicon detectors. UFSD have demonstrated the capability of achieving a precision of 30–35 ps, and to retain good performances up to fluences of $5 \cdot 10^{15}$ 1 MeV n_{eq} cm^{-2}. UFSD sensors are the detector chosen for the ATLAS and CMS timing layer, and they are currently produced by 3 foundries (CNM, FBK, and HPK). For environments with very high fluences, 3D trench detectors have been proposed as a viable alternative to UFSD.

Acknowledgments

We thank our collaborators within RD50, ATLAS and CMS who participated in the development of UFSD. Part of this work has been financed by the European Union Horizon 2020 Research and Innovation funding program, under Grant Agreement no. 654168 (AIDA-2020) and Grant Agreement no. 669529 (ERC UFSD669529), and by the Italian Ministero degli Affari Esteri and INFN Gruppo V, Italy. The work was supported by the United States Department of Energy, grant DE-FG02-04ER41286.

References

[1] G. Apollinari, O. Brning, T. Nakamoto, L. Rossi, Chapter 1: High Luminosity Large Hadron Collider HL-LHC. High Luminosity Large Hadron Collider HL-LHC, CERN Yellow Report (arXiv:1705.08830.5), 2017, 1–19. 21 p, 21 pages, chapter in High-Luminosity Large Hadron Collider (HL-LHC) : Preliminary Design Report. http://dx.doi.org/10.5170/CERN-2015-005.1. URL https://cds.cern.ch/record/2120673.

[2] S. Chatrchyan, et al., The CMS Experiment at the CERN LHC, JINST 3 (2008) S08004, http://dx.doi.org/10.1088/1748-0221/3/08/S08004.

[3] CMS Phase II Upgrade Scope Document, Tech. Rep. CERN-LHCC-2015-019. LHCC-G-165, CERN, Geneva (Sep 2015). URL https://cds.cern.ch/record/2055167.

[4] A. Airapetian, et al., The ATLAS experiment at the CERN large hadron collider, JINST 3 (08) (2008) S08003, URL http://stacks.iop.org/1748-0221/3/i=08/a=S08003.

[5] ATLAS Phase-II Upgrade Scoping Document, Tech. Rep. CERN-LHCC-2015-020. LHCC-G-166, CERN, Geneva (Sep 2015). URL https://cds.cern.ch/record/2055248.

[6] R. Yohay, Precision timing for the high luminosity upgrade of CMS, in: PoS 028, Pixel, 2017, URL https://pos.sissa.it/309/028/pdf.

[7] The LHCb Detector at the LHC, JINST 3 (08) (2008) S08005, URL http://stacks.iop.org/1748-0221/3/i=08/a=S08005.

[8] Expression of Interest for a Phase-II LHCb Upgrade: Opportunities in flavour physics, and beyond, in the HL-LHC era, Tech. Rep. CERN-LHCC-2017-003, CERN, Geneva (Feb 2017). URL http://cds.cern.ch/record/2244311.

[9] CMS, Technical Proposal for a MIP Timing Detector in the CMS Experiment Phase 2 Upgrade, Tech. Rep. CERN-LHCC-2017-027. LHCC-P-009, CERN, Geneva (Dec 2017). URL https://cds.cern.ch/record/2296612.

[10] H.F.-W. Sadrozinski, A. Seiden, N. Cartiglia, 4D tracking with ultra-fast silicon detectors, Rep. Progr. Phys. 81 (2) (2018) 026101, URL http://stacks.iop.org/0034-4885/81/i=2/a=026101.

[11] N. Cartiglia, et al., Design optimization of ultra-fast silicon detectors, Nucl. Instrum. Methods Phys. Res. A 796 (2015) 141–148.

[12] V. Sola, et al., Ultra-fast silicon detectors for 4D tracking, J. Instrum. 12 (2017) C02072.

[13] N. Cartiglia, et al., Beam test results of a 16 ps timing system based on ultra-fast silicon detectors, Nucl. Instrum. Methods Phys. Res. A 850 (2017) 83–88.

[14] W. Shockley, Currents to conductors induced by a moving point charge, J. Appl. Phys. 9 (1938) 635–636, http://dx.doi.org/10.1063/1.1710367.

[15] S. Ramo, Currents induced by electron motion, Proc. Ire. 27 (1939) 584–585, http://dx.doi.org/10.1109/JRPROC.1939.228757.

[16] G. Pellegrini, et al., Technology developments and first measurements of Low Gain Avalanche Detectors (LGAD) for high energy physics applications, Nucl. Instrum. Methods Phys. Res. A 765 (2014) 12–16.

[17] G.-F.D. Betta, et al., Design and tcad simulation of double-sided pixelated low gain avalanche detectors, Nucl. Instrum. Methods Phys. Res. A 796 (2015) 154–157.

[18] Z. Galloway, et al., Properties of HPK UFSD after neutron irradiation up to 6E15 n/cm2, (2017) arXiv:1707.04961.

[19] M. del Mar Carulla Areste, et al., Last measurements and developments on LGAD detectors [online] (TREDI2017, 2017).

[20] M. Ferrero, et al., Radiation resistant LGAD design, 2018. arXiv:1802.01745.

[21] M. Mandurrino, et al., Numerical simulation of charge multiplication in ultra-fast silicon detectors (ufsd) and comparison with experimental data, NSS/MIC IEEE Atlanta, 2017, submitted for publication IEEE Nuclear Transaction. URL https://www.eventclass.org/contxt_ieee2017/download/media?hash=2y13BYBKhVqHCribI5uxmX.JfufYlrAIVzhDJGSQOexR1eteDVyfn8yMK.

[22] M. Ferrero, et al., Developments in the Production of Ultra-Fast Silicon Detectors, NSS/MIC IEEE Atlanta, 2017.

[23] V. Sola, et al., First FBK Production of 50m Ultra-Fast Silicon Detectors, 2018. arXiv:1802.03988. URL https://inspirehep.net/record/1654651/files/1802.03988.pdf.

Please cite this article in press as: N. Cartiglia, et al., Timing layers, 4- and 5-dimension tracking, Nuclear Inst. and Methods in Physics Research, A (2018), https://doi.org/10.1016/j.nima.2018.09.157.

[24] S. Cadeddu, et al., A time-to-digital converter based on a digitally controlled oscillator, in: 2016 IEEE-NPSS Real Time Conference (RT), 2016, pp. 1–2, http://dx.doi.org/10.1109/RTC.2016.7543099.
[25] R. Giordano, et al., High-resolution synthesizable digitally-controlled delay lines, IEEE Trans. Nucl. Sci. 62 (6) (2015) 3163–3171, http://dx.doi.org/10.1109/TNS.2015.2497539.
[26] N. Neri, et al., 4d fast tracking for experiments at high luminosity lhc, J. Instrum. 11 (11) (2016) C11040, URL http://stacks.iop.org/1748-0221/11/i=11/a=C11040.
[27] Capeans, et al., ATLAS Insertable B-Layer Technical Design Report, Tech. Rep. CERN-LHCC-2010-013. ATLAS-TDR-19 (Sep 2010). URL https://cds.cern.ch/record/1291633.
[28] S. Parker, et al., Increased speed: 3d silicon sensors; fast current amplifiers, IEEE Trans. Nucl. Sci. 58 (2) (2011) 404–417, http://dx.doi.org/10.1109/TNS.2011.2105889.
[29] F. Cenna, et al., Weightfield2: A fast simulator for silicon and diamond solid state detector, Nucl. Instrum. Methods Phys. Res. A 796 (2015) 149–153, http://dx.doi.org/10.1016/j.nima.2015.04.015.

Please cite this article in press as: N. Cartiglia, et al., Timing layers, 4- and 5-dimension tracking, Nuclear Inst. and Methods in Physics Research, A (2018), https://doi.org/10.1016/j.nima.2018.09.157.